Biosensors and Bioelectronics 24 (2008) 356–361

Contents lists available at ScienceDirect

Biosensors and Bioelectronics

journal homepage: www.elsevier.com/locate/bios

Direct electrochemistry and electrocatalysis based on a film of horseradish peroxidase intercalated into Ni–Al layered double hydroxide nanosheets

Xu Chen, Chenglin Fu, Yi Wang, Wensheng Yang*, David G. Evans

State Key Laboratory of Chemical Resource Engineering, Beijing University of Chemical Technology, Beijing 100029, PR China

ARTICLE INFO

Article history:
Received 9 December 2007
Received in revised form 4 April 2008
Accepted 7 April 2008
Available online 16 April 2008

Keywords:
Direct electrochemistry
Electrocatalysis
Ni–Al LDH nanosheets
Horseradish peroxidase
Biosensor

ABSTRACT

Positively charged Ni–Al layered double hydroxide nanosheets (Ni–Al LDHNS) have been used for the first time as matrices for immobilization of horseradish peroxidase (HRP) in order to fabricate enzyme electrodes for the purpose of studying direct electron transfer between the redox centers of proteins and underlying electrodes. X-ray diffraction (XRD) and high-resolution transmission electron microscopy (HRTEM) revealed that the HRP–Ni–Al LDHNS film had an ordered structure and that HRP was intercalated into Ni–Al LDHNS with a monolayer arrangement. Field emission scanning electron microscopy (FESEM) showed that the HRP–Ni–Al LDHNS film had a uniform, porous morphology. UV–vis spectroscopy indicated that the intercalated HRP retained its native structure after incorporation in the Ni–Al LDHNS film. The immobilized HRP in Ni–Al LDHNS on the surface of a glassy carbon electrode (GCE) exhibited good direct electrochemical and electrocatalytic responses to the reduction of hydrogen peroxide (H_2O_2) and trichloroacetic acid (TCA). The resulting H_2O_2 biosensor showed a wide linear range from 6.00×10^{-7} M to 1.92×10^{-4} M, low detection limit (4.00×10^{-7} M) and good stability. The results show that Ni–Al LDHNS provide a novel and efficient platform for the immobilization of enzymes and realizing direct electrochemistry and that the materials have potential applications in the fabrication of third-generation biosensors.

1. Introduction

Direct electrochemistry of redox proteins has attracted considerable recent attention since it can serve as a model system to aid in the understanding of electron transfer mechanisms in biological systems, and also provide a foundation for the construction of third-generation biosensors and biofuel cells (Armstrong et al., 1988; Jia et al., 2002; Ivnitski et al., 2006). However, the electroactive centers of proteins are usually embedded within the macromolecule, and thus it is difficult for the direct electron transfer between the electroactive center and the electrode surface to occur. Moreover, the direct adsorption of proteins onto an electrode surface often results in their denaturation and consequent loss of electrochemical activity and bioactivity. Therefore, one of the main challenges in this area is to select a host matrix which can both provide a suitable microenvironment for proteins and also enhance direct electron transfer between the proteins and underlying electrodes (Yan et al., 2007; Xu et al., 2007). Various materials, such as polymer films (Huang et al., 2002; Liu and Hu, 2003), DNA film (Chen et al., 2000), nanomaterials (Zhang et al., 2004; Zong et al., 2006), and mesoporous silicates (Dai et al., 2005; Wu et al., 2007) have been used for this purpose. In general, inorganic materials are preferred to organic materials because of their intrinsic advantages such as possessing a regular structure, and good mechanical, chemical and thermal stabilities.

Of the wide variety of inorganic materials, layered materials are very attractive as support matrices for the immobilization of proteins (Kumar and Chaudhari, 2000; Wang et al., 2004). On the one hand, their open frameworks provide substrates with convenient access to the immobilized enzymes. On the other hand, the protective environment of the interlayer gallery can effectively inhibit microbial degradation, hydrolysis, and deamidation, and can extend the useful lifetime of the bound proteins (Peng et al., 2004). A variety of proteins have been immobilized within α-zirconium phosphates, layered niobates, layered titanate, and other layered hosts (Kumar and Chaudhari, 2002; Gao and Gao, 2007; Zhang et al., 2007a,b). For example, HRP immobilized in the galleries of layered α-zirconium phosphates have been shown to exhibit

* Corresponding author: Tel.: +86 10 64435271; fax: +86 10 64425385.
E-mail address: yangws@mail.buct.edu.cn (W. Yang).

0956-5663/$ – see front matter © 2008 Elsevier B.V. All rights reserved.
doi:10.1016/j.bios.2008.04.007

enhanced bioactivity and thermal stability (Kumar and Chaudhari, 2002). Modified electrodes formed by intercalation of myoglobin between layered titanate nanosheets were not only able to function in extreme pH environments, but also showed direct electrochemistry (Zhang et al., 2007a). However, the layers of these materials are negatively charged and, since proteins often bear an overall negative charge under physiological conditions, this limits their usefulness.

Layered double hydroxides (LDHs), also known as hydrotalcite-like materials or anionic clays, are available as both naturally occurring minerals and synthetic materials (Cavani et al., 1991). LDHs may be described by the general formula $[M^{II}_{1-x}M^{III}_{x}(OH)_2]^{x+}(A^{n-})_{x/n}\cdot mH_2O$. The host layer is of the brucite ($Mg(OH)_2$)-type, and partial substitution of divalent metal ions, M^{II}, by trivalent ones, M^{III}, yields an excess positive charge, x+, which is compensated by interlayer counteranions, A^{n-}. The positively charged layers are therefore able to immobilize negatively charged biomolecules. In addition, compared with other inorganic matrices, LDHs have a high versatility of chemical and physical–chemical properties, such as a wide range of possible chemical compositions, adjustable textural properties and preparation variables (Evans and Slade, 2005; Forano et al., 2006). These intrinsic properties make LDHs effective host structures for the immobilization of biomolecules (Choy et al., 1999; Ren et al., 2002; Barbosa et al., 2005). Some electrochemical biosensors based on LDHs as support matrices have been successfully developed, and shown to have remarkable catalytic performance, such as high sensitivity and a low Michaelis–Menten constant (Shan et al., 2003, 2004; Vial et al., 2006; Chen et al., 2007; Colombari et al., 2007). However, most of the previous work concerns LDH-mediated biosensors. To our knowledge, no previous studies have been reported of the heterogeneous direct electron transfer between the immobilized native redox proteins in LDHs and electrodes.

LDH nanosheets (LDHNS) have been recently synthesized by direct delamination of LDHs in the nitrate form (Li et al., 2005). Restacking of these nanosheets provides a simple and effective method of intercalating guest anions (especially macrobiomolecules) into LDHs. In this work, redox-active Ni–Al LDHNS were chosen as the host matrix and horseradish peroxidase (HRP) as a model redox protein. Ni–Al LDHNS were restacked by adding a solution of negatively charged HRP resulting in the intercalation of HRP into LDHs (referred to HRP–Ni–Al LDHNS). An HRP–Ni–Al LDHNS-modified electrode was fabricated by casting a suspension of HRP–Ni–Al LDHNS onto a glassy carbon electrode (GCE). The electrochemistry of the HRP–Ni–Al LDHNS/GCE was studied in detail. The electrocatalytic reduction of H_2O_2 and trichloroacetic acid (TCA) at the HRP–Ni–Al LDHNS/GCE was investigated and potential applications of the HRP–Ni–Al LDHNS/GCE as an unmediated electrochemical biosensor for the detection of H_2O_2 and TCA have been explored.

2. Experimental

2.1. Reagents

Horseradish peroxidase (HRP, 250 U mg^{-1}, p*I* 7.2) was purchased from Shanghai Lizhu Dongfeng Biotechnology Co. Ltd. (China). Poly(vinyl butyral) (PVB) was obtained from Sigma. Hydrogen peroxide (30% w/w) was from Beijing Chemical Engineering Plant. Dilute solutions of H_2O_2 were freshly prepared daily. All other chemicals were of analytical grade and used as received without further purification. Phosphate buffer solutions (PBS, 0.05 M) with various pH values were prepared by mixing stock standard solutions of Na_2HPO_4 and NaH_2PO_4. All aqueous solutions were prepared with deionized, doubly distilled water.

2.2. Synthesis of Ni–Al LDH nanosheets (Ni–Al LDHNS)

Ni–Al–NO_3 LDHs were synthesized by the coprecipitation method developed by (De Roy et al., 1992). All experiments were carried out under a stream of N_2 in order to avoid contamination by atmospheric CO_2. The delamination of Ni–Al–NO_3 LDHs was achieved by dispersing Ni–Al–NO_3 LDHs in formamide according to a published procedure (Li et al., 2005). Typically, Ni–Al–NO_3 LDHs (0.1 g) was mixed with 100 mL of formamide in a conical flask, which was sealed after purging with N_2 gas. The mixture was then agitated vigorously for about 3 h at 90 °C. After an appropriate centrifugation procedure (3000 rpm), a transparent, well-dispersed colloidal solution of exfoliated Ni–Al–NO_3 LDH (i.e. Ni–Al LDHNS) was obtained.

2.3. Preparation of HRP–Ni–Al LDHNS electrodes

Prior to coating, glassy carbon electrodes (GCE, diameter 3 mm) were polished successively with 1.0, 0.3, and 0.05 μm alumina powder, sonicated in doubly distilled water, and then dried with nitrogen. In order to bring about the intercalation of HRP into LDHNS, the suspension of HRP–Ni–Al LDHNS was prepared by mixing a stock solution of HRP (10 mg mL^{-1}, pH 7.5 PBS) with the colloidal solution of Ni–Al LDHNS (1 mg mL^{-1}) in a 1:1 volume ratio. The resulting suspension was stored at 4 °C in a refrigerator when not in use. In order to observe good cyclic voltammetric response, 3 μL of the suspension of HRP–Ni–Al LDHNS was dropped onto the surface of a GCE and allowed to dry at room temperature in order to obtain the HRP–Ni–Al LDHNS/GCE. Similarly, 3 μL of Ni–Al LDHNS (1 mg mL^{-1}) or HRP solution (5 mg mL^{-1}) was dropped on the surface of GCE to obtain the Ni–Al LDHNS/GCE or the HRP/GCE for comparison. The modified electrodes were dipped into an ethanol solution of PVB (1% w/v) for 1 min in order to enhance the adhesive ability and the stability of the film. The modified electrodes were stored at 4 °C in a refrigerator when not in use.

2.4. Apparatus

Electrochemical measurements were performed using a CHI 660B electrochemical workstation (Shanghai Chenhua Instrument Co., China). A conventional three-electrode system was used, including a modified electrode as working electrode, a platinum wire as auxiliary electrode, and an Ag/AgCl (3 mol L^{-1} KCl) electrode as reference electrode. The working solutions were purged with purified nitrogen for 20 min before measurement, and a nitrogen atmosphere was maintained over the solutions during the electrochemical measurements. All measurements were performed at room temperature.

Powder X-ray diffraction (XRD) patterns were recorded on a Rigaku D/MAX 2500 VB2+/PC X-ray diffractometer with Cu Kα radiation. Field emission scanning electron microscopy (FESEM) images were obtained with a Hitachi S4700 scanning electron microscope at an accelerating voltage of 20 kV. High-resolution transmission electron transfer microscopy (HRTEM) images were recorded on a Philips TECNAI F20 transmission electron microscope at an accelerating voltage of 200 kV. UV–vis experiments were performed with a Shimadzu UV-2501 PC spectrophotometer.

3. Results and discussion

3.1. Characterization of HRP–Ni–Al LDHNS film

Since the layers of LDHs are positively charged and HRP (p*I* 7.2) is negatively charged in pH 7.5 PBS, when the HRP solution and the Ni–Al LDHNS colloid are mixed the oppositely charged

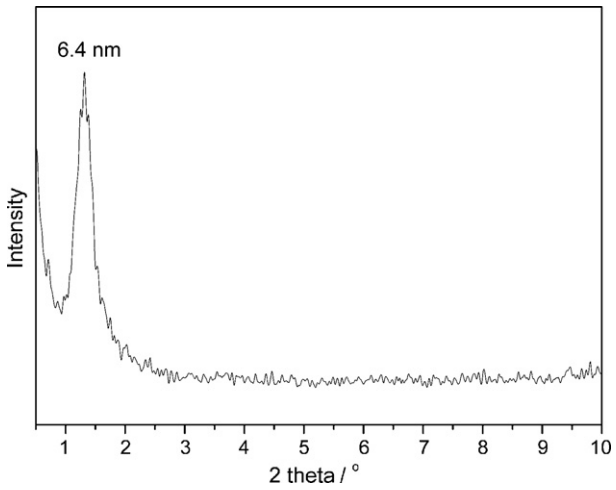

Fig. 1. Powder X-ray diffraction pattern of HRP–Ni–Al LDHNS film.

species should assemble due to electrostatic attraction. The XRD pattern of the HRP–Ni–Al LDHNS film shown in Fig. 1 suggests that the material has a layered structure with an interlayer spacing of 6.4 nm. The layer thickness of Ni–Al LDHNS is about 0.8 nm (the sum of the crystallographic thickness of the basal layer of LDHs (0.48 nm) and that of an adsorbed monolayer (0.3 nm) of formamide molecules) (Li et al., 2005), so that the gallery height is 5.6 nm. The observed interlayer distance correlates well with the size of HRP, 3.0 nm × 3.5 nm × 6.0 nm (Cai et al., 2006), and is somewhat larger than that observed (Zhang et al., 2007b) for HRP intercalated between layered titanate nanosheets (HRP–TNS, 4.65 nm). Such a large interlayer spacing should facilitate substrate access to the bound proteins. Moreover, the FWHM (full width at half of maximum intensity of the X-ray diffraction profile) of the XRD peak of HRP–Ni–Al LDHNS film is smaller than that for the HRP–TNS film (Zhang et al., 2007b), which can be taken to indicate that the distribution of HRP orientation is narrower (Peng et al., 2004). Such a distribution is important if the substrates are to effectively access the active sites of bound proteins (Kumar and Chaudhari, 2000). No diffraction peak was observed in the small-angle XRD pattern (not shown) of the Ni–Al LDHNS film formed without adding HRP. The XRD data therefore suggest that a monolayer of HRP was intercalated into Ni–Al LDHNS with a uniform orientation.

Fig. 2A shows a typical FESEM image of the HRP–Ni–Al LDHNS film which can be seen to be composed of slab-like crystals either dispersed or assembled to form three-dimensional particles. A similar morphology was observed for the composite formed by immobilizing hemoglobin (Hb) in the interlayer galleries of layered titanate (Wang et al., 2004). The uniform, porous three-dimensional film formed by HRP–Ni–Al LDHNS should facilitate access of substrates to the bound proteins. An HRTEM image of HRP–Ni–Al LDHNS, illustrated in Fig. 2B, shows HRP–Ni–Al LDHNS borders with the inorganic layers being clearly visible. The interlayer distance is approximately 6 nm, which is in agreement with the value of 6.4 nm determined by XRD.

UV–vis spectrometry is an effective technique to probe the characteristic structure of proteins. The position of the Soret absorption band of heme can provide some information about the denaturation of heme proteins and conformational changes of the heme group region (George and Hanania, 1953). Fig. S1 shows the UV–vis spectra of HRP under different conditions. No absorption was observed in the absence of HRP (Fig. S1a). The dry film cast from HRP–Ni–Al LDHNS on a glass slide showed a Soret band at 402 nm (Fig. S1c), which is nearly identical to that observed for a native HRP solution. This indicates that the HRP retains the essential features of its native structure after being immobilized in Ni–Al LDHNS.

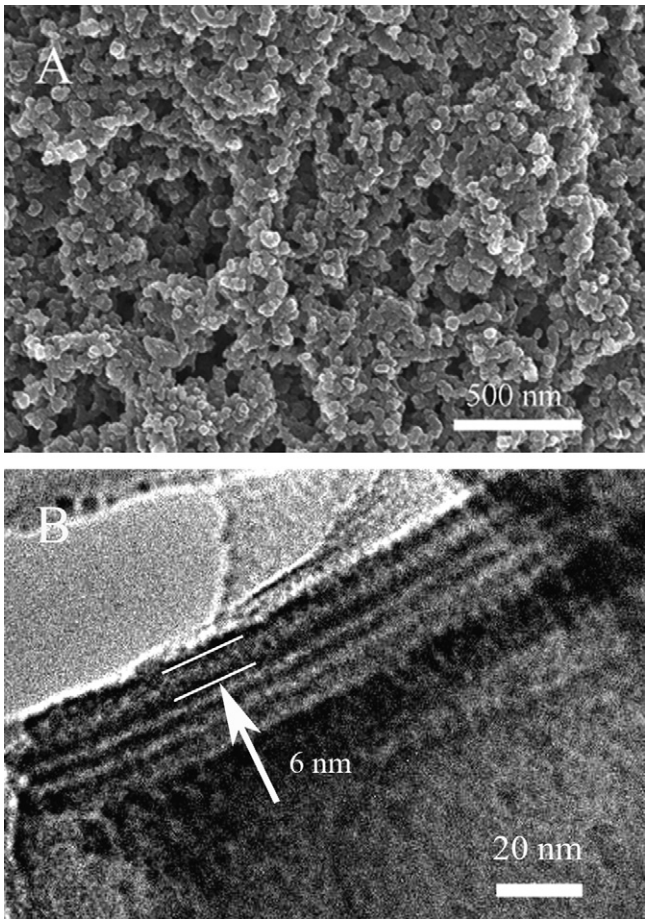

Fig. 2. (A) FESEM image of HRP–Ni–Al LDHNS film. (B) HRTEM image of HRP–Ni–Al LDHNS composite.

3.2. Direct electrochemistry of HRP–Ni–Al LDHNS/GCE

Fig. 3 shows the cyclic voltammograms (CVs) of different electrodes in 0.05 M PBS (pH 7.0) at 0.1 V s^{-1}. No obvious elec-

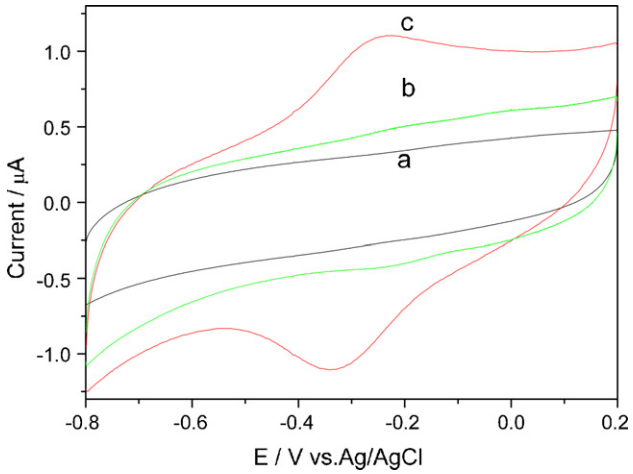

Fig. 3. CVs of Ni–Al LDHNS/GCE (a), HRP/GCE (b) and HRP–Ni–Al LDHNS/GCE (c) in 0.05 M PBS (pH 7.0) at a scan rate of 0.1 V s^{-1}.

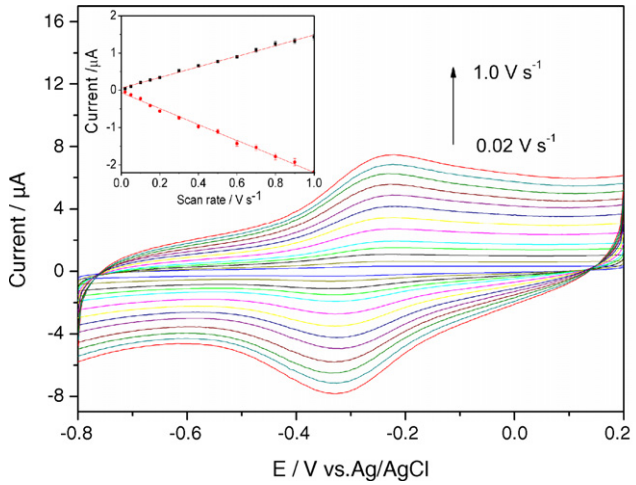

Fig. 4. CVs of HRP–Ni–Al LDHNS/GCE in 0.05 M PBS (pH 7.0) at scan rates of 0.02 V s^{-1}, 0.05 V s^{-1}, 0.1 V s^{-1}, 0.2 V s^{-1}, 0.3 V s^{-1}, 0.4 V s^{-1}, 0.5 V s^{-1}, 0.6 V s^{-1}, 0.7 V s^{-1}, 0.8 V s^{-1}, 0.9 V s^{-1} and 1.0 V s^{-1} (from inner to outer). Inset: plot of peak current vs. scan rate.

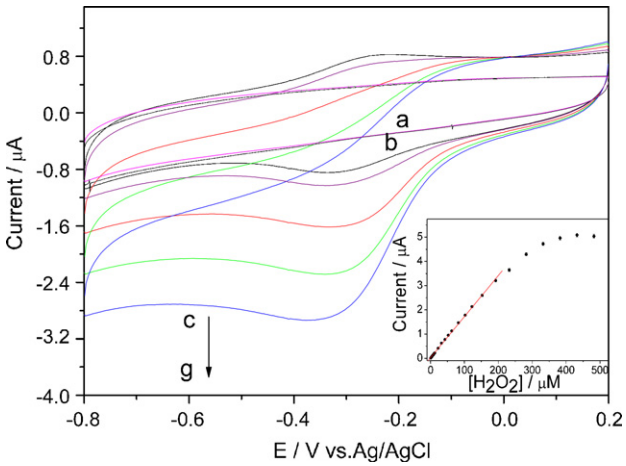

Fig. 5. CVs of Ni–Al LDHNS/GCE with 0 μM (a), 20 μM (b) H_2O_2 and CVs of HRP–Ni–Al LDHNS/GCE with 0 μM (c), 22.4 μM (d), 62.4 μM (e), 102.4 μM (f), 182.4 μM (g) H_2O_2 in 0.05 M PBS (pH 7.0) at a scan rate of 0.1 V s^{-1}. Inset: plot of catalytic peak current vs. H_2O_2 concentration for the HRP–Ni–Al LDHNS/GCE.

trochemical response was observed for either Ni–Al LDHNS/GCE (Fig. 3a) or HRP/GCE (Fig. 3b). However, the HRP–Ni–Al LDHNS/GCE gave a couple of well-defined quasi-reversible redox peaks at −0.256 V and −0.334 V (Fig. 3c), corresponding to the reduction and oxidation of the electroactive center of the immobilized HRP. This may be attributed to the HRP intercalated into LDHNS having an appropriate orientation to facilitate direct electron transfer between the electroactive center of HRP and the GCE. The formal potential ($E^{0'}$) of the HRP–Ni–Al LDHNS/GCE, calculated from the average value of the anodic and cathodic peak potentials, is −0.295 V vs. Ag/AgCl (−0.096 V vs. NHE) in 0.05 M pH 7.0 PBS, which agrees well with the values obtained for HRP–chitosan (−0.091 V vs. NHE) (Huang et al., 2002), HRP–gluten (−0.091 V vs. NHE) (Liu and Hu, 2003), and HRP–AQ (−0.090 V vs. NHE) (Huang and Hu, 2003) film modified electrodes in a pH 7.0 buffer. This suggests that the majority of HRP molecules preserve their native structure after being intercalated into LDHNS and that the interlayer galleries of LDHNS can provide a biocompatible microenvironment similar to biopolymers. The potential difference between the two current peaks (ΔE_p), 78 mV, is lower than that for HRP–TNS (Zhang et al., 2007b). The small value of ΔE_p can be attributed to the immobilized HRP molecules having a uniform orientation (Li and Dong, 1997; Xiao et al., 2000), which is consistent with the XRD analysis.

The effect of varying the scan rate on the electrochemical response of the HRP–Ni–Al LDHNS film is shown in Fig. 4. The anodic and cathodic peak currents were found to be linearly proportional to the scan rate. The peak current was proportional to the scan rate over the range from 0.02 V s^{-1} to 1.0 V s^{-1} as shown in the inset of Fig. 4, indicating a surface-controlled process. From the peak-to-peak separation of the CVs at scan rates ranging from 0.05 V s^{-1} to 0.5 V s^{-1}, the average electron transfer rate constant k_s of HRP immobilized in the Ni–Al LDHNS film was estimated to be 3.36 s^{-1}, according to the model of Laviron (Laviron, 1979) using the formula $k_s = mnFv/RT$, where n is the number of electrons transferred, F is Faraday's constant, m is a parameter related to the peak-to-peak separation, v is the scan rate, R is the gas constant, and T is the temperature. Here, $T = 298$ K and $n = 1$. The observed value is larger than those of 1.13 s^{-1} for HRP immobilized in DNA film (Chen et al., 2000), 0.92 s^{-1} for HRP immobilized on a hexagonal mesoporous silica matrix (Dai et al., 2005), and 0.66 s^{-1} for HRP coated on a graphite electrode (Ruzgas et al., 1995). This indicates that the Ni–Al LDHNS facilitates electron transfer between HRP and the electrode. From the integration of the reduction peak of the HRP–Ni–Al LDHNS/GCE at different scan rates, the average surface concentration of HRP was calculated to be 6.80×10^{-11} mol cm^{-2}, which is larger than the theoretical monolayer coverage (2×10^{-11} mol cm^{-2}). This suggests that multi-layer of immobilized HRP in the Ni–Al LDHNS film participate in the electron transport process.

The influence of varying the solution pH on the CV peak position was also investigated. The peak potentials of HRP were found to depend strongly on the solution pH (Fig. S2). Increasing the pH of the solution (from 5.0 to 9.0) resulted in a linear negative shift of the formal potential with a slope of −42.4 mV pH^{-1}, which is similar to that reported for HRP immobilized in grafted zirconia nanoparticle–collagen hybrid materials (Zong et al., 2006). The value is reasonably close to the theoretical value of −59.0 mV pH^{-1} at 25 °C expected for a reversible, one-proton coupled single-electron transfer process (Bond, 1980). Thus, the electrode reaction in the HRP–Ni–Al LDHNS film can be expressed as

$$\text{HRP–Fe(III)} + \text{H}^+ + \text{e}^- \rightleftarrows \text{HRP–Fe(II)} \quad (1)$$

3.3. Electrocatalytic properties of HRP–Ni–Al LDHNS/GCE

The electrocatalytic reduction of H_2O_2 at the HRP–Ni–Al LDHNS/GCE was studied by cyclic voltammetry. Fig. 5 shows the CVs both in the presence and absence of H_2O_2 at the Ni–Al LDHNS/GCE and the HRP–Ni–Al LDHNS/GCE in pH 7.0 PBS. No peak was observed at the Ni–Al LDHNS/GCE in the presence of H_2O_2 in the potential range 0.2 V to −0.8 V (curve b in Fig. 5). However, at the HRP–Ni–Al LDHNS/GCE, the reduction peak current increased after the addition of H_2O_2, and the oxidation peak current simultaneously decreased, indicating the characteristic of the electrocatalytic activity of HRP in the reduction of H_2O_2. The reduction peak current increased with the concentration of H_2O_2 in solution (curves c–g in Fig. 5). A linear relationship of electrocatalytic reduction peak current and H_2O_2 concentration was observed in the concentration range 6.00×10^{-7} M to 1.92×10^{-4} M (inset in Fig. 5). The calibration equation can be expressed as i (μA) = 0.0272 + 0.0167c (μM) with a correlation coefficient of 0.999 ($n = 18$). The HRP–Ni–Al LDHNS/GCE showed a detection limit of 4.00×10^{-7} M (S/N = 3) for biosensing of H_2O_2. Compared with HRP immobilized in a TiO_2 nanoparticle film (Zhang et al., 2004), a TNS film (Zhang et al., 2007b) and cationic aluminosilicate clays (Li and Hu, 2003), the HRP–Ni–Al

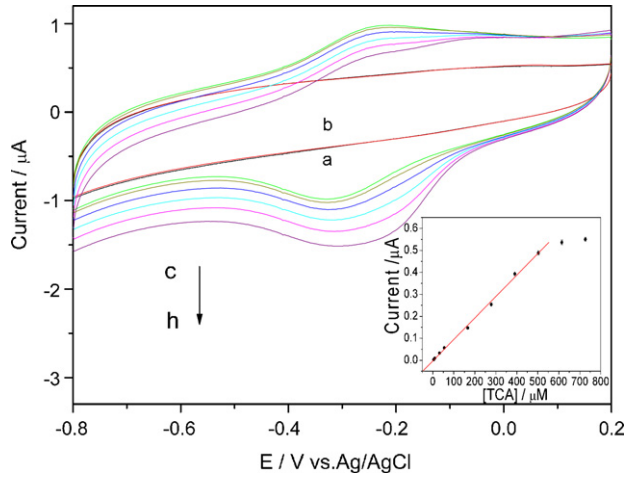

Fig. 6. CVs of Ni–Al LDHNS/GCE with 0 μM (a), 22.2 μM (b) TCA and CVs of HRP–Ni–Al LDHNS/GCE with 0 μM (c), 32.6 μM (d), 166.7 μM (e), 278.7 μM (f), 390.7 μM (g), 726.7 μM (h) TCA in 0.05 M PBS (pH 7.0) at a scan rate of 0.1 V s^{-1}. Inset: plot of catalytic peak current vs. TCA concentration for the HRP–Ni–Al LDHNS/GCE.

LDHNS/GCE has a wider linear detection range and lower detection limit. The reason may be that HRP effectively retains its bioactivity after immobilization in Ni–Al LDHNS, and the large interlayer galleries of the matrix and three-dimensional porous structure of the film result in a very low mass transport barrier. When the concentration of H_2O_2 was higher than 3.32×10^{-4} M, the catalytic current tended to level off, suggesting a typical Michaelis–Menten process. The apparent Michaelis–Menten constant (K_M^{app}), obtained from the electrochemical version of the Lineweaver–Burk equation, was 0.262 ± 0.005 mM. This value is smaller than those for HRP immobilized in grafted zirconia nanoparticle–collagen hybrid materials (Zong et al., 2006) and in TNS films (Zhang et al., 2007b). The low K_M^{app} value can be taken to indicate facile access and high affinity of H_2O_2 to the active site of the immobilized HRP.

The electrocatalytic reduction of TCA at the HRP–Ni–Al LDHNS/GCE was also investigated by cyclic voltammetry (Fig. 6). On addition of TCA to the solution, an increase in the reduction peak current at about −0.334 V was seen, accompanied by a decrease in the oxidation peak current. No redox peak was observed at the Ni–Al LDHNS/GCE under the same conditions (curve b in Fig. 6). The reduction peak current at the HRP–Ni–Al LDHNS/GCE increased with the concentration of TCA (curves c–h in Fig. 6). These results are characteristic of electrochemical catalysis. A linear relationship between the catalytic reduction peak current and the concentration of TCA was obtained in the concentration range 9.90×10^{-6} M to 5.02×10^{-4} M (inset in Fig. 6). The calibration equation can be expressed as $i\,(\mu A) = -0.00282 + 0.000976c\,(\mu M)$ with a correlation coefficient of 0.999 ($n = 8$).

3.4. Real sample analysis

As an example of a real sample, the concentration of H_2O_2 in commercial eyedrops was determined using the biosensor. The sample was diluted with doubly distilled water in order to give a concentration of H_2O_2 in the detection limit range. The concentration of H_2O_2 was calculated to be (0.886 ± 0.004) M, which is very close to the actual concentration specified by the manufacturers (0.882 M). This suggests that the HRP–Ni–Al LDHNS/GCE biosensor should be reliable and effective in practical determinations of H_2O_2.

The concentration of TCA added to tap water was also determined using the biosensor. 100 μM TCA was added to a tap water sample. The average recovery of the biosensor was 103% ($n = 4$). The tap water sample without added TCA did not show a detectable signal. The possible interference of foreign matter, which might occur in real samples, was investigated. When the concentrations of Fe^{3+}, SO_4^{2-}, ascorbic acid, Cl^- and ClO_3^- in the sample were 10 times that of TCA, no significant interference was observed. However in the presence of the same concentration of phenol, the peak current showed an increase of approximately 10%. A PbO_2 coating on the surface of the modified electrodes could remove the interference of phenol in the sample.

3.5. Stability and reproducibility of HRP–Ni–Al LDHNS/GCE

The stability of the HRP–Ni–Al LDHNS/GCE was initially evaluated by examining the cyclic voltammetric peak currents of HRP after continuously scanning for 100 cycles. The voltammetric response remained almost unchanged, indicating that the enzyme electrode was stable in the buffer solution. The operational stability of the enzyme electrode in a continuous operation mode at room temperature was also studied. The response of the enzyme electrode to 20 μM H_2O_2 decreased by 8.0% of the initial response after 5 h, and the sensibility decreased by 7.1% of its initial value. When the enzyme electrode was not used, it was stored at 4 °C in a dry state. The electrode was tested weekly. It retained 93.0% of its initial current response to H_2O_2 after a month. The good stability can be attributed to three factors: (1) LDHNS contains a large number of hydroxyl groups, which help to maintain the activity of the enzyme (Li et al., 1998) and can form strong hydrogen bonds with polar functional groups of the biomolecules which helps to stabilize the bound enzyme (Vial et al., 2006; Barhoumi et al., 2006). (2) The positively charged LDHNS effectively immobilizes the negatively charged HRP because the strong electrostatic interactions prevent the enzyme from leaking out of the film. (3) The rigid galleries of the layered inorganic matrix provide a confined space, which may impose an additional barrier to protein denaturation (Peng et al., 2004; Zhou and Dill, 2001). In addition, the reproducibility of the HRP–Ni–Al LDHNS/GCE was also examined for an H_2O_2 concentration of 20 μM; five enzyme electrodes from the same batch showed an acceptable reproducibility with a relative standard deviation of 5.0%.

4. Conclusions

HRP has been intercalated into Ni–Al LDHNS by delamination and restacking, and the direct electron transfer between the intercalated HRP and the underlying electrode was studied for the first time. XRD and HRTEM revealed that the HRP–Ni–Al LDHNS film involves an ordered layered structure with a monolayer of HRP intercalated between LDHNS. An FESEM image showed that the HRP–Ni–Al LDHNS film was uniform and porous. UV–vis spectroscopy confirmed that HRP intercalated into Ni–Al LDHNS retains its native secondary structure. Due to the good biocompatible microenvironment and the suitable orientation provided by Ni–Al LDHNS, direct electrochemistry of the intercalated HRP was realized. The HRP–Ni–Al LDHNS/GCE showed good electrocatalytic activity in the reduction of both H_2O_2 and TCA. The resulting biosensor showed excellent analytical performance in the determination of H_2O_2, with wider linear range, lower detection limit, smaller K_M^{app} value and better stability than previously reported materials. These characteristics all suggest that Ni–Al LDHNS is an effective support matrix and suitable for protein immobilization. The HRP–Ni–Al LDHNS film should have potential application in the fabrication of third-generation biosensors. The exciting properties of HRP–Ni–Al LDHNS nanocomposites suggest that the intercalation of other enzymes into LDHNS may lead to wide and promising applications in biocatalysis and biosensors.

Acknowledgments

This work was supported by the National Natural Science Foundation of China (No. 20705004), the National 863 Project (No. 2006AAO3Z343), the 111 Project (No. B07004) and the Young Scholars Fund of Beijing University of Chemical Technology (No. QN0621).

Appendix A. Supplementary data

Supplementary data associated with this article can be found, in the online version, at doi:10.1016/j.bios.2008.04.007.

References

Armstrong, F.A., Hill, H.A.O., Walton, N.J., 1988. Acc. Chem. Res. 21, 407–413.
Barbosa, U.A.S., Ferreira, A.M.D.C., Constantino, V.R.L., 2005. Eur. J. Inorg. Chem. 8, 1577–1584.
Barhoumi, H., Maaref, A., Rammah, M., Martelet, C., Jaffrezic, N., Mousty, C., Vial, S., Forano, C., 2006. Mater. Sci. Eng. C 26, 328–333.
Bond, A.M., 1980. Modern Polarographic Methods in Analytical Chemistry. Marcel Dekker, New York, pp. 29–30.
Cai, W.Y., Xu, Q., Zhao, X.N., Zhu, J.J., Chen, H.Y., 2006. Chem. Mater. 18, 279–284.
Cavani, F., Trifirò, F., Vaccari, A., 1991. Catal. Today 11, 173–301.
Chen, H., Mousty, C., Cosnier, S., Silveira, C., Moura, J.J.G., Almeida, M.G., 2007. Electrochem. Commun. 9, 2240–2245.
Chen, X.H., Ruan, C.M., Kong, J.L., Deng, J.Q., 2000. Anal. Chim. Acta 412, 89–98.
Choy, J.H., Kwak, S.Y., Park, J.S., Jeong, Y.J., Portier, J., 1999. J. Am. Chem. Soc. 121, 1340–1399.
Colombari, M., Ballarin, B., Carpani, I., Guadagnini, L., Mignani, A., Scavetta, E., Tonelli, D., 2007. Electroanalysis 19, 2321–2327.
Dai, Z.H., Ju, H.X., Chen, H.Y., 2005. Electroanalysis 17, 862–868.
De Roy, A., Forano, C., El Malki, K., Bess, J.P., 1992. In: Occelli, M.L., Robson, H.E. (Eds.), Synthesis of Microporous Materials, Expanded Clays and Other Microporous Solids. Van Nostrand Reinhold, New York, pp. 108–169.
Evans, D.G., Slade, R.C.T., 2005. Struct. Bond. 119, 1–87.
Forano, C., Vial, S., Mousty, C., 2006. Curr. Nanosci. 2, 283–294.
Gao, L., Gao, Q.M., 2007. Biosens. Bioelectron. 22, 1454–1460.
George, P., Hanania, G., 1953. Biochem. J. 55, 236–243.
Huang, H., Hu, N.F., Zeng, Y.H., Zhou, G., 2002. Anal. Biochem. 308, 141–151.
Huang, R., Hu, N.F., 2003. Biophys. Chem. 104, 199–208.
Ivnitski, D., Branch, B., Atanassov, P., Apblett, C., 2006. Electrochem. Commun. 8, 1204–1210.
Jia, J.B., Wang, B.Q., Wu, A.G., Cheng, G.L., Li, Z., Dong, S.J., 2002. Anal. Chem. 74, 2217–2223.
Kumar, C.V., Chaudhari, A., 2000. J. Am. Chem. Soc. 122, 830–837.
Kumar, C.V., Chaudhari, A., 2002. Chem. Commun., 2382–2383.
Laviron, E., 1979. J. Electroanal. Chem. 101, 19–28.
Li, B., Niu, L., Kou, W., Deng, Q., Dong, S.J., 1998. Anal. Biochem. 256, 130–132.
Li, J.H., Dong, S.J., 1997. J. Electroanal. Chem. 431, 19–22.
Li, L., Ma, R.Z., Ebina, Y.S., Iyi, N.B., Sasaki, T., 2005. Chem. Mater. 17, 4386–4391.
Li, Z., Hu, N.F., 2003. J. Electroanal. Chem. 558, 155–165.
Liu, H.Y., Hu, N.F., 2003. Anal. Chim. Acta 481, 91–99.
Peng, S.G., Gao, Q.M., Wang, Q.G., Shi, J.L., 2004. Chem. Mater. 16, 2675–2684.
Ren, L.L., He, J., Zhang, S.C., Evans, D.G., Duan, X., 2002. J. Mol. Catal. B: Enzym. 18, 3–11.
Ruzgas, T., Gorton, L., Emméus, J., Marko-Varga, G., 1995. J. Electroanal. Chem. 391, 41–49.
Shan, D., Cosnier, S., Mousty, C., 2003. Anal. Chem. 75, 3872–3879.
Shan, D., Cosnier, S., Mousty, C., 2004. Biosens. Bioelectron. 20, 390–396.
Vial, S., Forano, C., Shan, D., Mousty, C., Barhoumi, H., Martelet, C., Jaffrezic, N., 2006. Mater. Sci. Eng. C 26, 387–393.
Wang, Q.G., Gao, Q.M., Shi, J.L., 2004. J. Am. Chem. Soc. 126, 14346–14347.
Wu, S.B., Ju, H.X., Liu, Y., 2007. Adv. Funct. Mater. 17, 585–592.
Xiao, Y., Ju, H.X., Chen, H.Y., 2000. Anal. Biochem. 278, 22–28.
Xu, J.M., Li, W., Yin, Q., Zhong, H., Zhu, Y.L., Jin, L.T., 2007. J. Colloid Interface Sci. 315, 170–176.
Yan, R., Zhao, F.Q., Li, J.W., Xiao, F., Fan, S.S., Zeng, B.Z., 2007. Electrochim. Acta 52, 7425–7431.
Zhang, L., Zhang, Q., Li, J.H., 2007a. Adv. Funct. Mater. 17, 1958–1965.
Zhang, L., Zhang, Q., Lu, X.B., Li, J.H., 2007b. Biosens. Bioelectron. 23, 102–106.
Zhang, Y., He, P.L., Hu, N.F., 2004. Electrochim. Acta 49, 1981–1988.
Zhou, H.X., Dill, K.A., 2001. Biochemistry 40, 11289–11293.
Zong, S.Z., Cao, Y., Zhou, Y.M., Ju, H.X., 2006. Langmuir 22, 8915–8919.